RSC Advances

PAPER

Cite this: *RSC Adv.*, 2015, **5**, 7880

Facile and low-cost approach towards a PVDF ultrafiltration membrane with enhanced hydrophilicity and antifouling performance *via* graphene oxide/water-bath coagulation

Tengfei Wu,[a] Baoming Zhou,[a] Ting Zhu,[a] Jie Shi,[a] Zhiwei Xu,*[a] Chuansheng Hu[a] and Jiajun Wang*[b]

Addressed herein is a facile and low-cost approach to endow hydrophobic polyvinylidene fluoride (PVDF) membranes with reliable hydrophilicity and antifouling properties. Porous asymmetric hydrophilic membranes with tunable morphology were facilely fabricated *via* phase inversion using an aqueous solution of graphene oxide (GO) as the coagulation bath. An increment in pore size and surface roughness was observed for membranes treated by a GO/water-coagulation bath (GB). The bovine serum albumin rejection of GB-treated membranes increased by 38.99% when the concentration of GO in the coagulation bath was 0.5 g L^{-1}. The contact angle of membranes decreased from 75.9° to 58.8° and the water flux increased by 140% when the dosage of GO was 2 g L^{-1}. Furthermore, fouling resistances of membranes revealed that GB-treated membranes had a higher flux recovery ratio (85.7%) than pristine PVDF (43.3%). Meanwhile, the protein adsorption of GB-treated membranes was decreased by 69.3% compared with that of pristine PVDF membranes. The cost of the membranes can be lowered by using a GB approach compared with GO-mixed matrix membranes because of the reusability of GO in a coagulation bath. This research presents an effective method to tailor membrane performance *via* GB rather than embedding GO in the membrane matrix.

Received 30th October 2014
Accepted 23rd December 2014

DOI: 10.1039/c4ra13476a

www.rsc.org/advances

1. Introduction

Over the past few decades, ultrafiltration technology has attracted plentiful attention on account of its effective purification and concentration of oil–water separation and protein effluent separation in many membrane separation and filtration processes.[1–3] It is generally accepted that the porous structure and hydrophilicity of membranes play crucial roles in membrane manufacturing processes.[4] An appropriate porous membrane should be excellent in permeability, hydrophilicity and chemical resistance to the feed streams. An asymmetric membrane is a very good option for high permeability.[5] Polyvinylidene fluoride (PVDF) is extensively used to form such an asymmetric membrane with regard to its excellent thermal stability, chemical resistance and mechanical properties.[6–8] Nevertheless, the intrinsic hydrophobic property of PVDF often causes severe membrane fouling and decline of permeability, which is a major challenge for the widespread application in water and wastewater treatments.[6]

Many researches have been investigated to tailor the performance of PVDF membranes *via* surface modification or blending modification.[6,9] Among various modification techniques, blending modification has an advantage of easy preparation by phase inversion. The most significant factor, which affects the phase inversion path of a membrane forming system, is the composition of the casting solution and the coagulation media.[5,10]

In recent years, substantial studies on casting solution modifications have engaged in blending of inorganic nanomaterials with casting solution. Various inorganic nanoparticles such as Al_2O_3,[11] SiO_2,[12] TiO_2,[13] ZrO_2,[14] Fe_3O_4,[15] $LiOCl_4$,[16] ZnO[17] and $BaTiO_3$ [18] were used to fabricate organic–inorganic hybrid membranes. It has been shown that the introduction of inorganic nanoparticles can tailor the morphology, reduce the compaction, enhance the permeability and improve the antifouling performance of membranes.[19–22] However, the introduction of nanoparticles into polymeric membranes have some shortcomings such as the aggregation/dispersion behavior control due to surface interactions and the inevitable loss of nanoparticles during the preparation process.[19,23]

[a]*State Key Laboratory of Hollow Fiber Membrane Materials and Processes, School of Textiles, Tianjin Polytechnic University, Tianjin 300387, People's Republic of China. E-mail: xuzhiwei@tjpu.edu.cn; Fax: +86 22 83955231; Tel: +86 22 83955231*

[b]*Photon Sciences Directorate, Brookhaven National Laboratory, Building 744, Upton, New York 11973, USA. E-mail: jjwang@bnl.gov; Fax: +1-631-344-8822; Tel: +1-631-344-8822*

In addition to the composition of casting solution, adjusting coagulation bath condition is considered to be another efficient and facile approach to tailor the performance of porous phase inversion membranes.[24,25] Ahmad *et al.*[26] fabricated a PVDF flat sheet membrane by immersing into various concentrations of ethanol in water as the coagulation bath and the hydrophibicity of the membranes was improved. Sukitpaneenit *et al.*[27] used a series of non-solvents such as methanol to obtain membranes with controlled morphology and good mechanical property. Teow *et al.*[28] found that PVDF/TiO_2 mixed-matrix membranes with 0.01 g L^{-1} of TiO_2 in the coagulation bath exhibited extraordinary permeability with superior retention properties of humic acid. Graphene oxide (GO), which possesses strong hydrophilicity due to the presence of numerous functional groups (*e.g.*, carboxyl, carbonyl, hydroxyl, and epoxy groups),[29] high specific surface area and fascinating chemical properties, can be an ideal candidate of additive for polymeric membrane.[30–40] Although it has been demonstrated that the hydrophilicity and permeability of PVDF membranes can be improved obviously by introduction of GO, the poor solubility of GO in most of the solvents makes them hard to obtain effective dispersion in bulk solution.[34,36,37] On the contrary, the existence of abundant oxygen-containing functional groups makes GO nanosheets be capable of dispersing in water to yield a prolonged, stable suspension easily.[35,41] In addition, GO can cause thermodynamic exchange rate between non-solvent and solvent due to the high affinity of GO towards non-solvent water during the phase inversion,[42] which is expected to embed and deposit on the surface of the membrane along with the non-solvent (GO/water) exchange during phase separation. What's more, GO in coagulation bath can be retrieved for cyclic utilization while GO for casting solution modification is retained in mixed matrix membranes along with the membranes preparation, therefore the cost of membranes can be lower compared with GO-mixed matrix membranes because of the reusability of GO in coagulation bath. Keeping these in view, the present work was designed.

Thus, based on the above considerations, in the present work we have focused our attention on the effect of GO concentration in GO/water-coagulation bath on the hydrophilicity, morphology, permeability and antifouling performance of PVDF membranes fabricated by the immersion phase inversion method. To the best of our knowledge, the use of GO in the coagulation bath to fabricate PVDF ultrafiltration membranes has not been reported yet.

2. Experimental

2.1. Materials

PVDF (FR-904), as the membrane material, was supplied by Shanghai 3F New Materials Co., Ltd. Polyvinyl pyrrolidone (PVP) and *N*,*N*-dimethylacetamide (DMAc) were the products of Tianjin Kermel Chemical Co., Ltd. Graphite powder was purchased from Qingdao Ruisheng Graphite Co., Ltd. Bovine serum albumin (BSA, M_w = 68 000) was obtained from Beijing Biohao Biotechnology Co., Ltd.

2.2. Preparation and characterization of GO

Graphite oxide was synthesized by an modified Hummers' approach,[43] where graphite flakes (3 g) was added to a mixture of concentrated H_2SO_4–H_3PO_4 (360 mL/40 mL), then $KMnO_4$ (18 g) was slowly added while stirring. The resulting mixture was stirred for 24 h at 50 °C. Afterwards, the reactants were cooled to ambient temperature and poured onto an ice bath with small amount of H_2O_2 (~400 mL). The dispersion was centrifuged down and rinsed several times with 5% HCl aqueous solution, then by deionized water until neutral pH. Finally, graphite oxide with different concentrations (0.5, 1 and 2 g L^{-1} based on the volume of water) was exfoliated to achieve well-dispersed GO solutions under ultrasonication for 3 h.[33] To determine chemical compositions of GO, Fourier-transform infrared spectroscopy (FTIR) was performed.

2.3. Preparation of membranes

The PVDF ultrafiltration membranes were fabricated *via* the phase inversion process. Typically, PVDF (15 g) and PVP (1 g) was dissolved in DMAc (84 g) at 50 °C and then stirred for 24 h to generate a homogenous casting solution. After releasing the air bubbles, the solution was spread onto a glass plate and horizontally dipped into GO/water-coagulating bath (GB) at ambient temperature. Upon complete coagulation, the resultant membranes were preserved in deionized water before characterization tests. The prepared membranes were labeled as PVDF, PVDF-GB-0.5, PVDF-GB-1, PVDF-GB-2, respectively, and the numbers indicated the concentration of GO in the coagulation bath (0.5, 1 and 2 g L^{-1}).

2.4. Characterization of membranes

The surface morphology of membranes was observed with a scanning electron microscope (SEM; S-4800, Hitachi, Japan). With an atomic force microscope (AFM; CSPM5500, China), the surface roughness of membranes were investigated. Roughness parameters such as the root mean square (R_q), mean surface roughness (R_a) and the height difference between the highest peak and the lowest valley (R_z) were quantified with a scanning range of 10 μm × 10 μm. The crystal phase was determined by X-ray diffraction (XRD, Bruker D8 Discover) with Cu Kα radiation (1.54059 Å). The water contact angle of membranes was measured using a contact angle goniometer (JC2000D1, China). The membrane porosity ε (%) was calculated by gravimetric method[21] and mean pore size r_m (nm) was determined using Guerout–Elford–Ferry equation[44] based on the data of porosity and pure water flux. To minimize the experimental error, all the reported values were the average values of at least five replicates.

2.5. Permeation flux and rejection of membranes

Permeation flux and rejection of membranes were tested by the ultrafiltration experimental system with an effective membrane area of 19.63 cm^2. The permeation tests were directed at 25 °C with a feed pressure of 0.1 MPa. Prior to the permeation testing, the membranes were compacted at 0.15 MPa for 1 h to reach a steady flux, and then the flux was measured at 0.1 MPa. After

this, the rejection tests were performed using BSA solutions (1 g L^{-1}). The water flux, J (L m^{-2} h^{-1}) and BSA rejection, R (%), were estimated by eqn (1) and (2), respectively:

$$J = \frac{Q}{A \times T} \quad (1)$$

$$R = \left(1 - \frac{C_P}{C_F}\right) \times 100\% \quad (2)$$

where Q is the total volume penetrating through the membrane (L) during the operation time T (h) with an effective filtration area of A (m^2). C_P and C_F respectively represent the concentrations of BSA in permeation and feed solutions.

2.6. Antifouling properties of membranes

To survey the fouling behaviors of membranes, the flux recovery rate (FRR) was introduced and evaluated according to the following definition:[21]

$$FRR = \frac{J_{w1}}{J_{w2}} \times 100\% \quad (3)$$

where J_{w1} and J_{w2} are the water flux of the original membrane and cleaned membrane after filtration process, respectively.

Obviously, higher FRR demonstrates superior antifouling property. Also, in order to explore the fouling mechanism in details, the total fouling ratio (R_t), reversible fouling ratio (R_r) and irreversible fouling ratio (R_{ir}) are determined as follows:[45]

$$R_t = \left(1 - \frac{J_p}{J_{w1}}\right) \times 100\% \quad (4)$$

$$R_r = \left(\frac{J_{w2} - J_p}{J_{w1}}\right) \times 100\% \quad (5)$$

$$R_{ir} = \left(\frac{J_{w1} - J_{w2}}{J_{w1}}\right) \times 100\% = R_t - R_r \quad (6)$$

Static protein adsorption test was also carried out with BSA aqueous solution to estimate the fouling resistant property of membranes and the measurements were conducted following the procedure according to the literature.[22] The recorded values were average of at least 5 replicates for each membrane.

3. Results and discussion

3.1. FTIR and XRD of membranes

Fig. 1 showed the FTIR spectra of GO and the investigated membranes. The most prominent features of GO spectrum (Fig. 1e) were the adsorption peaks at 3432 cm^{-1} and 1678 cm^{-1} which corresponded to the hydroxyl groups and carboxyl groups, respectively. Furthermore, the peaks at 1770 cm^{-1} and 1071 cm^{-1} corresponded with the stretching vibration of carbonyl and the antisymmetric stretching vibration of epoxy bond, respectively. These findings indicated the existence of the hydroxyl groups and carboxyl groups of GO, which were consistent with the findings described in previous reports.[46] The polar oxygen-containing groups can easily combine with water

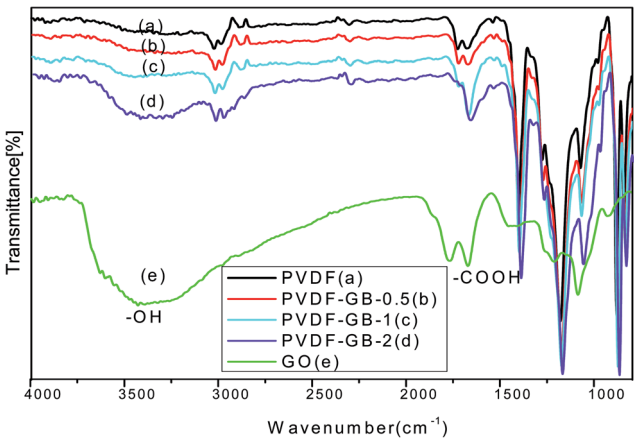

Fig. 1 FTIR spectra of (a) pristine PVDF membrane, (b–d) the GB-treated membranes and (e) GO.

to form hydrogen bond, which would improve the membrane hydrophilicity. Fig. 1a showed the FTIR spectrum of the pristine PVDF membrane. The peaks at 3021, 1401 and 1178 cm^{-1} can be ascribed to the stretching and deformation vibrations of CH_2 and the CF_2 stretching vibration, respectively.[30] These peaks also appeared in the spectra of the GB-treated membranes (Fig. 1b–d). Comparing with pristine PVDF membrane, the GB-treated membranes had wider and intenser peaks at 3426 cm^{-1}, which indicated that the surface hydrophilicity was obviously improved.

The XRD patterns of PVDF and PVDF-GB-2 were shown in Fig. 2. A sharp peak around 10° in the XRD pattern of PVDF-GB-2 was associated with the (001) inter-layer structure of GO sheets. The XRD peaks of PVDF at 18.2° and 26.5° were related to the α phase and the peak around 20.2° was attributed to the β phase. In PVDF-GB-2, the intensity of the (110) peak at 20.4° significantly increased compared to that of PVDF, indicating that there are interactions between polymer and GO which influenced the PVDF crystal structure (transition of phase) in the membrane. Therefore, it was hypothesized that there were a

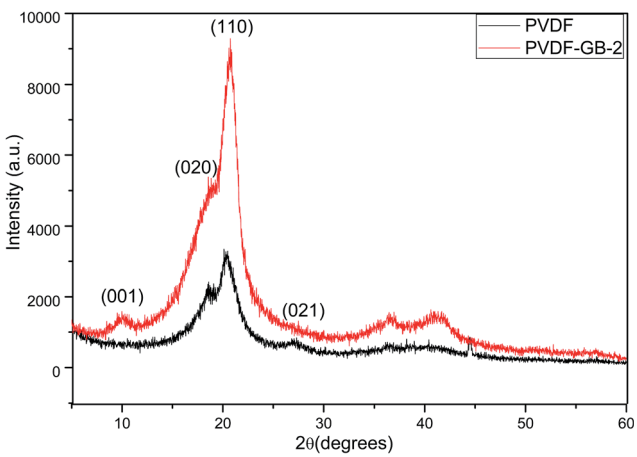

Fig. 2 XRD patterns of pristine PVDF membrane and PVDF-GB-2 membrane.

few GO sheets deposited on the surface of the membrane probably due to the interaction between the –C═O groups in GO and the $-CF_2$ groups in PVDF,[47,48] which facilitated the hydrophilicity of membranes.

3.2. Morphology of membranes

SEM and AFM were carried out to investigate effect of GB on the morphological changes of PVDF ultrafiltration membranes. Fig. 3 presented the SEM images and the three-dimensional AFM images of membranes. Obviously, a significant improvement in surface porosity can be observed visually from the SEM pictures. Larger pores appeared on the GB-treated membrane surface compared with pristine PVDF membranes, which may play a favorable role on membrane flux. The experimental results can be ascribed to the improved membrane hydrophilicity and increased pore size of surface causing thermodynamic solvent–nonsolvent exchange rate during the phase inversion.[42]

Moreover, the roughness parameters of membrane surface were presented in Table 1, which was acquired from investigating five randomly selected AFM images with the AFM analysis software. It was revealed that the GB-treated membranes presented larger roughness parameters than pristine PVDF membranes. The root-mean-squared (R_q) surface roughness and the mean surface roughness (R_a) for PVDF-GB-0.5, PVDF-GB-1 and PVDF-GB-2 were 27.12%, 39.41%, 38.28% and 26.11%, 33.21%, 36.06% higher than those of pristine PVDF membranes, respectively. The results would be in favor of the enhancement of membrane hydrophilic property since it is well known that the hydrophilic surface had smaller water contact angle as the surface roughness was higher in some range.[49] The increase of membrane roughness was on account of the increased pore size on membrane surface owing to the quicker liquid–liquid phase separation, which was in accordance with changes in permeability and separation performance depicted in the later part.

To further analyze the membrane surface topography, the SEM images with higher magnification of pristine PVDF membrane and GB-treated membrane (PVDF-GB-1) were obtained. As depicted in Fig. 4, a rougher surface of GB-treated membrane with more porosity can be observed visually compared to the corresponding pristine PVDF membrane. The phenomenon of poriness and roughness — where GB-treated membrane showed a ridge- and valley-surface texture and a higher porosity — was highly in accordance with the overall porosity and roughness information of membranes presented in Table 1.

The overall porosity information of membranes was exhibited in Table 1. As could be seen from Table 1, the porosity of GB-treated membranes was in a range of 75–83% while pristine PVDF membranes possessed a porosity of 60.71%. Furthermore, the mean pore size of GB-treated PVDF membranes was also improved. Owing to the rapid phase demixing of phase separation process, surface with a high total porosity and a large pore formed at the membrane skin layer. Correspondingly, GB-treated membranes rendered a favorable porous surface, which was undeniably good for promoting membrane permeability.

3.3. Hydrophilicity of membranes

The surface hydrophilicity of membranes was evaluated by water contact angle based on the sessile drop technique. Generally, lower water contact angle refers to stronger hydrophilicity. On solid surface, water contact angle attenuates gradually with time due to capillary absorption and the wetting process, and the contact angle decaying strongly depended upon the hydrophilicity of membranes.[50] As depicted in Fig. 5, the original contact angle of pristine PVDF membrane was about 81°, and it declined to 71.5° after 120 s, which implied the poor hydrophilicity of pristine PVDF membrane. Relative to that of pristine PVDF membrane, there was an apparent change in the water contact angle for PVDF-GB-0.5 and PVDF-GB-1, with 15° and 16° reductions in the contact angle after 120 s, respectively. The PVDF-GB-2 contact angle was remarkably smaller (25° reductions), showing enhanced hydrophilicity in comparison with those of the other membranes.

Also, to further confirm the hydrophilicity of the membranes, advancing and receding water contact angle was measured (Fig. 5). Generally, the more hydrophilic the membrane is, the larger the discrepancy between advancing and receding contact angle. From the comparisons among the static, advancing, and receding contact angles in Fig. 5, it was obvious that the discrepancy in initial static contact angle (or advancing contact angle) and receding contact angle was enlarged for all the GB-treated membranes. According to the water contact angle measurements, it could be concluded that the hydrophilicity of the GB-treated membranes can be improved and this hydrophilicity improvement should certainly benefit the fouling resistance and permeability of membranes.

The increased hydrophilicity of membranes could be interpreted as follows. Immersion process of the casting solution into the coagulation bath is a demixing process and the membrane structure depends on the rate of demixing process.[51] Instantaneous demixing favors to the formation of macrovoids, whereas delayed demixing often terminates to a denser structure.[52] It has been proved that the hydrophilicity of PVDF membranes was influenced by porous surfaces and roughness of membranes,[26] which was discussed in an earlier part. On the one hand, higher porosity of membrane surface can reduce the contact angle of water drops on membrane surface, which has been proven by Omidvar[53] and Ulbricht.[54] On the other hand, it has been shown that the contact angle of a hydrophobic surface increases with increasing surface roughness, whereas the contact angle of a hydrophilic surface decreases with increasing roughness.[55,56] However, if the increase in roughness is caused by the deposition of hydrophilic GO sheets on the membrane surface, it improves the membrane surface hydrophilicity significantly although the roughness is high.[11] Consequently, the improved hydrophilicity played a remarkable role on the flux and antifouling properties of membranes, which would be discussed at length in subsequent part.

3.4. Permeation flux and rejection of membranes

For the water flux and BSA rejection evaluation, dead-end flow measurements were performed and the results were shown in

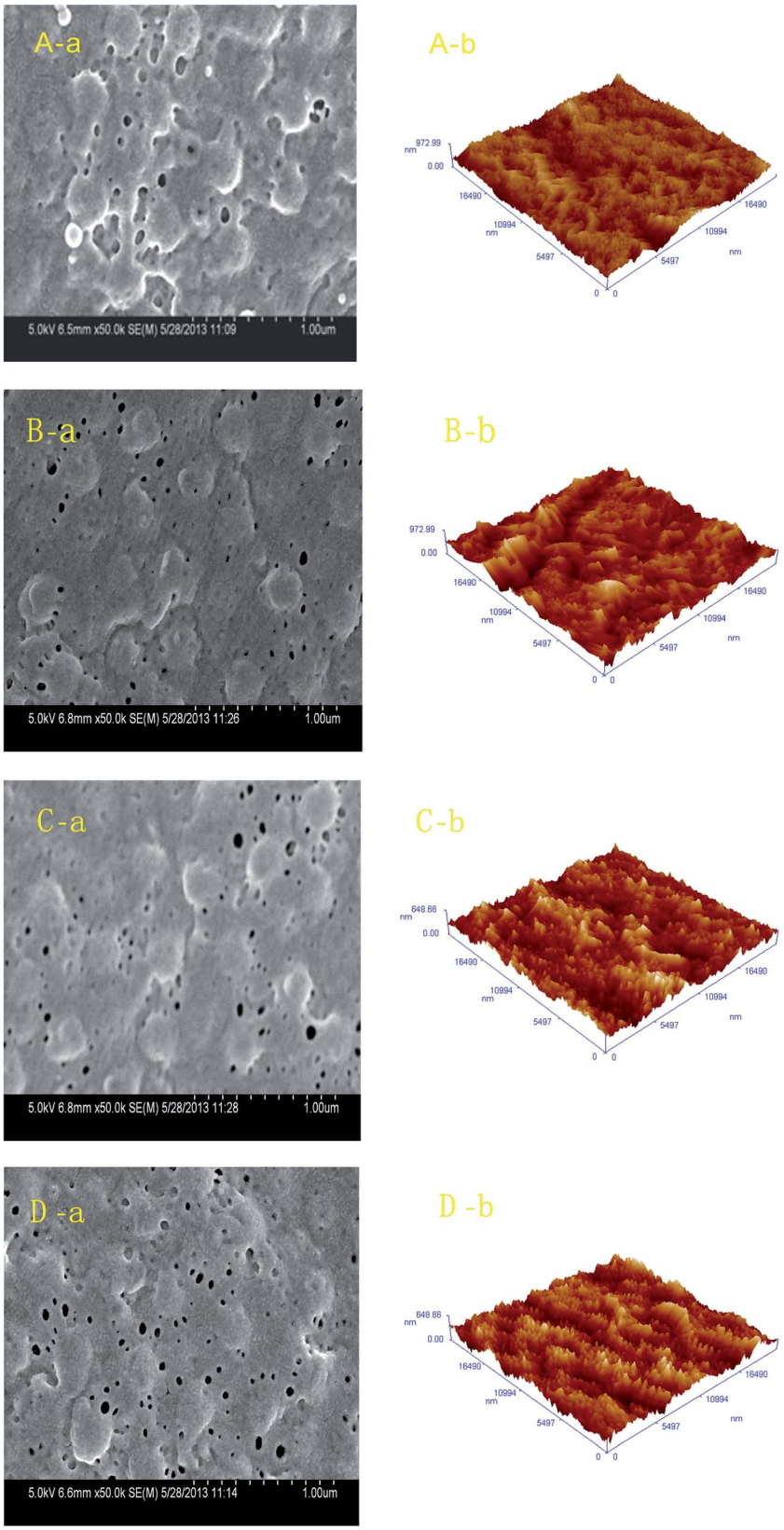

Fig. 3 Typical surface SEM photographs and three-dimensional AFM photographs for (A) PVDF, (B) PVDF-GB-0.5, (C) PVDF-GB-1 and (D) PVDF-GB-2.

Table 1 Porosity, surface mean pore size and roughness parameters for membranes PVDF, PVDF-GB-0.5, PVDF-GB-1 and PVDF-GB-2 membranes

Membranes	Porosity (%)	Average diameter (nm)	Surface area (μm^2)	Roughness		
				R_a (nm)	R_q (nm)	R_z (nm)
PVDF	60.71	81.0	522.6	56.3	70.8	528
PVDF-GB-0.5	75.08	85.5	562.4	71.0	90.0	741
PVDF-GB-1	81.80	88.1	537.3	75.0	98.7	776
PVDF-GB-2	83.11	91.2	559.5	76.6	97.9	778

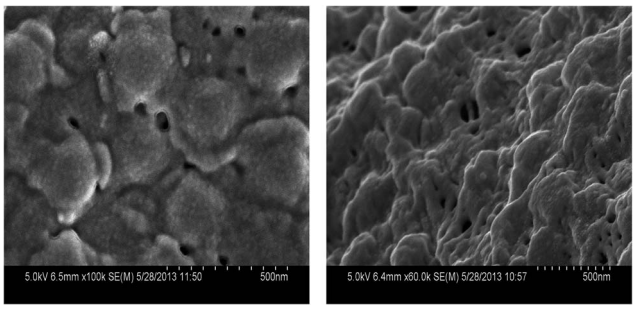

Fig. 4 Surface SEM images with higher magnification of PVDF (Left) and PVDF-GB-1 (Right).

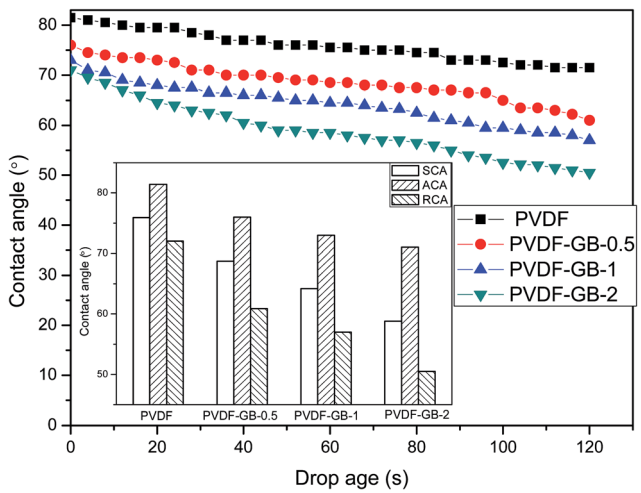

Fig. 5 The curves of water contact angle decaying with drop age for pristine PVDF and GB-treated membranes (PVDF-GB-0.5, PVDF-GB-1 and PVDF-GB-2). Inset are the comparisons of advancing contact angle (ACA), receding contact angle (RCA) and static contact angle (SCA) of membranes.

Fig. 6. As expected, water flux tended to increase with increasing GO content in coagulation bath. When GO content was 2 g L^{-1}, water flux reached its peak value of 467.75 L m^{-2} h^{-1} and increased 140% compared to that of pristine PVDF membrane. This improvement in water flux may be the compromise between two major membrane characteristics: (i) from the data of water contact angle (Fig. 5), it can be seen that the hydrophilicity of GB-treated membranes increased with increasing

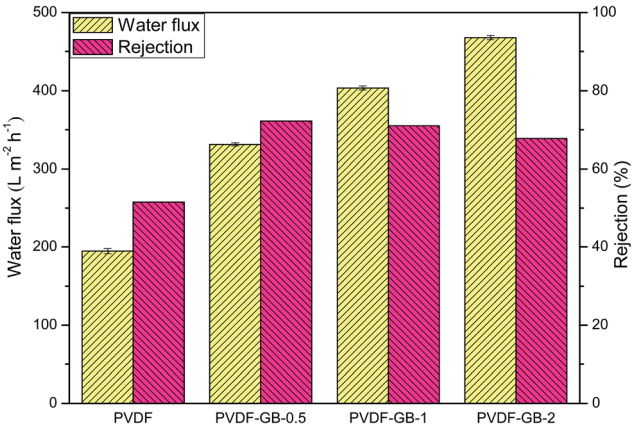

Fig. 6 Pure water flux and BSA rejection of PVDF, PVDF-GB-0.5, PVDF-GB-1 and PVDF-GB-2.

GO content in coagulation bath, which could attract water molecules within the membrane matrix and hence improve the water permeability.[57] (ii) The quick exchange between non-solvent and solvent across the interface generated a high porosity and accelerated the transportation of water. Furthermore, as displayed in Table 1, the average pore diameters of membranes increased with GO content in coagulation bath. The order to the mean pore size of membrane surface was consistent with the order of the water flux, implying that the pore size of membranes also contributed to the improvement of pure water flux. Conclusively speaking, the hydrophilicity and structure (pore size and porosity) of membranes account for enhancing the pure water flux of membranes. The increased hydrophilicity and enlarged pore size lead to an increase in water permeation through membranes.

The results of BSA rejection ratio were also depicted in Fig. 6. Compared with the BSA rejection of pristine PVDF membrane (51.8%), the value of PVDF-GB-0.5, PVDF-GB-1 and PVDF-GB-2 was enhanced by 38.99%, 36.92% and 30.42%, respectively. The increase in BSA rejection of GB-treated membranes can be ascribed to a combination of two factors. Firstly, as could be seen in Fig. 3, all of GB-treated membranes had dense outer surfaces, which contacted with protein solutions and could dominate the extent of protein retention primarily.[58] Secondly, the decrease in hydrophobic interaction between hydrophilic membrane surface and BSA protein might be responsible for slight increment of BSA rejection. Thereby, GB-treated

membranes were endowed higher rejection than pristine PVDF membrane. So it was the combined action of pore size and interface interaction that led to the phenomenon that the BSA rejection of PVDF-GB-2 with larger pore size was slightly lower than that of PVDF-GB-0.5 and PVDF-GB-1 though PVDF-GB-2 possessed the best hydrophilicity.

3.5. Antifouling properties of membranes

To survey the antifouling properties of membranes, the dynamic filtration operations were conducted and the results were presented in Fig. 7. Typical time dependent flux of membranes was recorded and the result was shown in Fig. 7a. The filtration operations included three stages. The first stage was referred to half hour pure water permeation. The second stage was 1 h of BSA solution ultrafiltration and the third stage was the pure water flux of cleaned membranes washed with distilled water for another half an hour. In the first stage, the initial flux for PVDF-GB-0.5, PVDF-GB-1 and PVDF-GB-2 surpassed that of pristine PVDF membrane. When the pure water alternated with BSA solution, the flux decreased dramatically due to protein adsorption and/or convective deposition on membrane surface.[59] Generally, the flux decline in the protein filtration is ruled over by membrane fouling and concentration polarization. With a rapid stirring on membrane surface, the concentration polarization can be restricted effectively.[21] Therefore, we settled the stirring rate of protein solution at 400 rpm to anticipate a negligible concentration polarization. Hence, the membrane fouling was the main culprit of the reduction in flux. From the data of last stage, we could see that the pure water flux was recovered in different degrees after membrane cleaning and cannot completely resume at the initial value due to entrapment of proteins within the pores. Based on the obtained flux, FRR was estimated using eqn (3), and the results were displayed in Fig. 7b.

Fig. 7b illustrated FRR value which was calculated to assess the extent of flux recovery after BSA fouling. Higher FRR indicates superior antifouling property of membrane. FRR of pristine PVDF membrane was only 43.3%, implying a poor

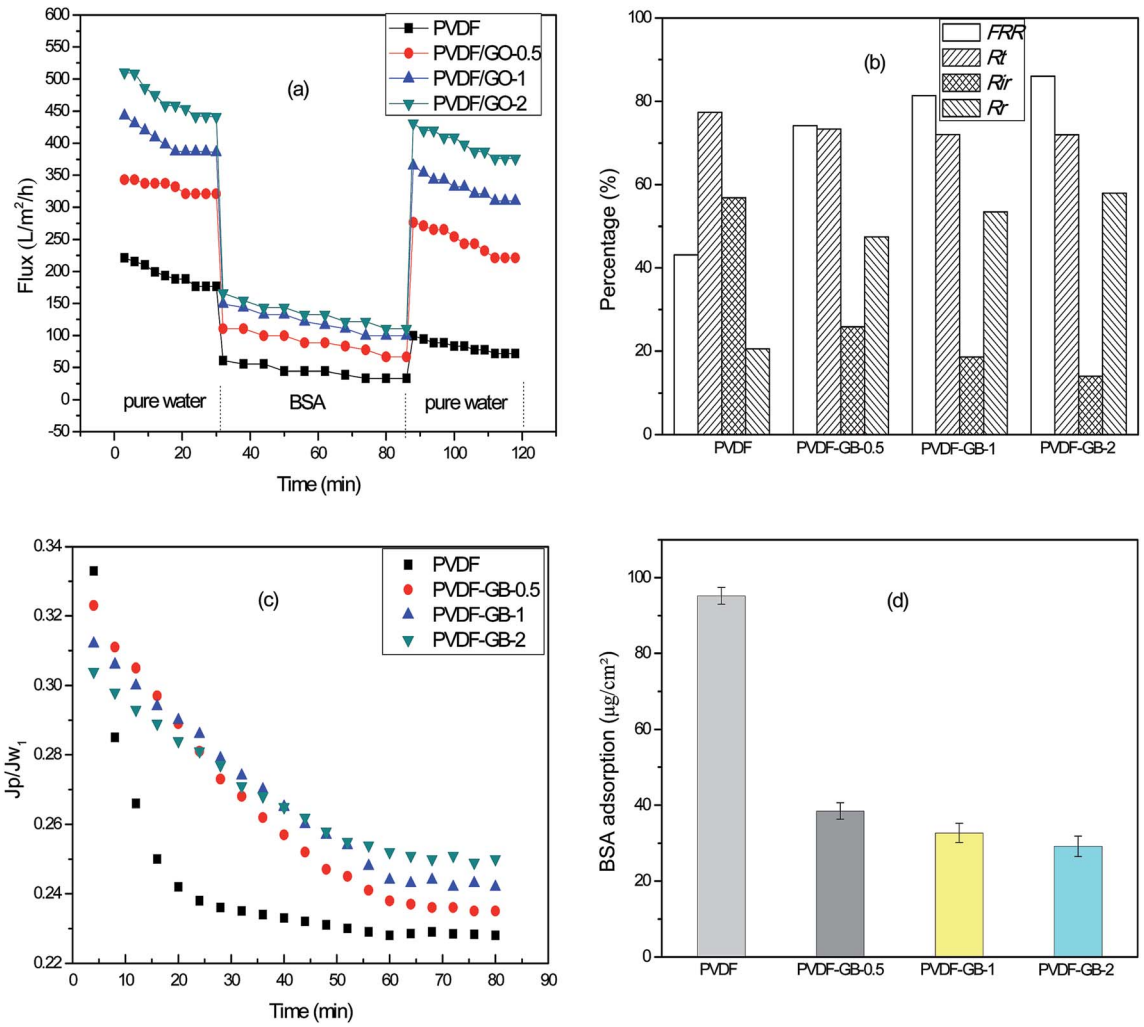

Fig. 7 The antifouling properties of membranes. (a) Flux *versus* time for membranes at 0.1 MPa during three steps: water flux for 30 min, BSA solution flux for 60 min, and water flux for 30 min after 20 min washing with distilled water; (b) water flux recovery and fouling resistance ratio of membranes; (c) normalized flux of membranes; (d) BSA adsorption of membranes.

Table 2 Comparison of the comprehensive performance for GO-mixed matrix membranes reported in the literature and GB-treated membranes in this work

Membrane	Optimum dosage of GO	Contact age (°)	Water flux (L m^{-2} h^{-1})	BSA rejection (%)	Water flux recovery (%)	Reference
PVDF-GO	0.2%[a]	60.7	457.9	91.1	96.4	30
PVDF-GO	1%[a]	68.1	505.0	87.0	—	31
PVDF-GO	1%[a]	66.4	173.0	83.7	85.1	32
PVDF-GO	2%[a]	60.5	26.5	—	88.6	39
PVDF-GO	1%[a]	62.0	361.2	55.0	—	36
PVDF-GB	2 g L^{-1}[b]	58.8	467.8	67.6	85.7	This work

[a] The GO nanosheets based on the weight of PVDF (g g^{-1}). [b] The concentration of GO nanosheets in GO/water coagulation bath.

antifouling property. FRR of GB-treated membranes was obviously higher than that of pristine PVDF membrane. In the best case, related to PVDF-GB-2 membrane, FRR of the membrane was 85.7%. The observed trend of FRR was matched by hydrophilicity of membranes (see Fig. 5). Hydrophilic surface can adsorb water molecules and generate a hydration layer, which retards the contaminant adsorptions within the membrane.[60]

In fact, membrane fouling was mainly related to protein deposition on the surface or entrapment within the pores (irreversible resistance) and the loose protein adsorption on membrane surface (reversible resistance).[37] As shown in Fig. 7b, R_t of GB-treated membranes, which was the sum of R_r and R_{ir}, was slightly lower compared to pristine PVDF membrane. R_{ir} of pristine PVDF membrane was 56.8% (more than 73% in total fouling). However, R_{ir} of GB-treated membranes dramatically decreased and the irreversible fouling percentage in total fouling declined to 35.2%, 25.8% and 19.5% of PVDF-GB-0.5, PVDF-GB-1 and PVDF-GB-2, indicating that the antifouling property of GB-treated membranes was remarkably enhanced. In summary, FRR and R_r of GB-treated membranes were improved and the results for these phenomena would be interpreted in detail later.

Moreover, the antifouling properties of GB-treated membranes could be estimated through the ratio of BSA solution flux (J_p) and pure water flux (J_{w1}). The more dramatically the curve declined, the more seriously membrane fouled.[39] As shown in Fig. 7c, for pristine PVDF membrane, the ratio of J_p and J_{w1} declined remarkably in the first 30 min, and then tended to stable, but GB-treated membranes glided gradually and kept stable until 60 min. The slow change of flux ratio demonstrated superior antifouling properties due to increased hydrophilicity of membranes.

Protein adsorption is also an important indicator to measure the protein resistance of membranes and the results of static BSA adsorption were shown in Fig. 7d. A large amount of BSA was adsorbed on pristine PVDF membrane surface, while the adsorbed amount of BSA decreased significantly for GB-treated membranes. For PVDF-GB-2, the average amount of adsorbed BSA decreased to 29.2 μg cm^{-2}, only 30.7% of pristine PVDF membrane (95.1 μg cm^{-2}). The results showed that the BSA adsorption of GB-treated membranes could be reduced apparently, and the protein resistance of GB-treated membranes was thereby improved. It was widely accepted that a hydrophilic membrane would adsorb water molecules and form a hydration layer and steric hindrance on the surface of membranes, which could consequently inhibit protein adsorption of BSA.[39]

Several factors such as hydrophilicity, surface charge and surface roughness have influence on the membrane fouling process, during which the hydrophobic force (entropy effect), hydrogen bonding, electrostatic force (Coulomb force) and van der Waals forces contribute to the membrane fouling.[61] As is shown in Fig. 7b, the sequence of FRR and total fouling resistance was in line with the membrane hydrophilicity (Fig. 5). The results suggested the antifouling capability of GB-treated PVDF membranes was improved significantly. The increased hydrophilicity of membranes could induce a water layer and impede protein molecules from binding to surface.[60] These results accorded with those of static BSA adsorption (Fig. 7d).

In addition, although it generally deemed that ultrafiltration membranes with high surface roughness will be fouled easily due to stacking of contaminants at the valley and ridge structure,[9] opposite viewpoint has also been voiced that membrane with a rough surface could markedly enhance the membrane hydrophilicity and thus lessen the interaction of membrane surface and foulants.[11] The drastic improvement of hydrophilicity can form hydrogen bonds between water molecules and membrane surface,[60] making hydrophobic proteins hard to approach the surface of membranes. Accordingly, protein fouling can be reduced effectively. In our experiments, membrane surface roughness was measured with three-dimensional AFM images (Fig. 3) and the roughness parameters were exhibited in Table 1. Compared with pristine PVDF membrane, the surface roughness of GB-treated membranes increased. The mean surface roughness of membranes increased from 56.3 (PVDF) to 71.0 nm, 75.0 and 76.6 nm for PVDF-GB-0.5, PVDF-GB-1 and PVDF-GB-2 membranes, respectively. As aforesaid, an increase in the surface roughness of membranes does not play a negative role on membrane property, but rather it significantly enhances the antifouling properties.

Conclusively speaking, the GB-treated membranes show tremendous potential in hydrophilicity and antifouling properties. In addition, after a deep investigation listed in Table 2, it

is inspiring to compare contact angle, water flux, BSA rejection and water flux recovery of GO-mixed matrix membranes reported in previous literature with those of GB-treated membranes in this work. Compared with GO-mixed matrix membranes, the cost of GB-treated membranes can be lower due to the reusability of GO in coagulation bath while the hydrophilicity and antifouling properties remained fairly. It is indicated that the GO/water-coagulation bath approach may have the potential to replace the GO-mixed method in enhancing the hydrophilicity, permeability and antifouling properties of PVDF ultrafiltration membranes.

4. Conclusions

In this work, porous asymmetric hydrophilic membranes with tunable morphology were facilely fabricated *via* the phase inversion process using a GO/water-coagulation bath. GO concentration in GO/water-coagulation bath played a favorable role on the characteristics of PVDF membranes and the effects were enumerated as below:

(1) The GB-treated membranes exhibited higher mean pore size, porosity and roughness than pristine PVDF membranes.

(2) The static contact angle dropped from 75.9° (PVDF) to 68.7°, 64.2° and 58.8° for PVDF-GB-0.5, PVDF-GB-1 and PVDF-GB-2, respectively, which indicated a significant enhancement of membrane hydrophilicity.

(3) The pure water flux of GB-treated membranes increased by 140% (PVDF-GB-2) and the BSA rejection of PVDF-GB-0.5, PVDF-GB-1 and PVDF-GB-2 was enhanced by 38.99%, 36.92% and 30.42%, respectively, compared with pristine PVDF membranes.

(4) The GB-treated membranes showed lower protein adsorption along with higher flux recovery ratio and fouling resistance compared with pristine PVDF membranes, indicating that GB-treated membranes had better antifouling properties than pristine PVDF membranes.

In summary, the study presents a facile and low-cost approach to endow hydrophobic PVDF membranes with reliable hydrophilicity and antifouling properties *via* a GO/water-coagulation bath approach rather than embedding GO in membrane matrix. Compared with GO-mixed matrix membranes, the cost of GB-treated membranes can be lower due to the reusability of GO in coagulation bath while the hydrophilicity and antifouling properties of membranes remained fairly. The GO/water-bath coagulation approach may have the potential to replace the GO-mixed method in improving the performance of PVDF ultrafiltration membranes.

Acknowledgements

The work was funded by the National Natural Science Foundation of China (11175130) and the Petrochemical Joint Funds of National Natural Science Fund Committee – China National Petroleum Corporation (U1362108).

References

1 J. Mansouri, S. Harrisson and V. Chen, *J. Mater. Chem.*, 2010, **20**, 4567–4586.
2 Y. S. Li, L. Yan, C. B. Xiang and L. J. Hong, *Desalination*, 2006, **196**, 76–83.
3 C. Lee, S. Bae, S. Han and L. Kang, *Desalination*, 2007, **202**, 239–246.
4 Q. Yang, N. Adrus, F. Tomicki and M. Ulbricht, *J. Mater. Chem.*, 2011, **21**, 2783–2811.
5 S. J. Oh, N. Kim and Y. T. Lee, *J. Membr. Sci.*, 2009, **345**, 13–20.
6 F. Liu, N. A. Hashim, Y. Liu, M. Abed and K. Li, *J. Membr. Sci.*, 2011, **375**, 1–27.
7 Y. Sui, Z. Wang, X. Gao and C. Gao, *J. Membr. Sci.*, 2012, **413–414**, 38–47.
8 M. Zhang, Q. T. Nguyen and Z. Ping, *J. Membr. Sci.*, 2009, **327**, 78–86.
9 D. Rana and T. Matsuura, *Chem. Rev.*, 2010, **110**, 2448–2471.
10 A. Rahimpour and S. Madaeni, *J. Membr. Sci.*, 2007, **305**, 299–312.
11 L. Yan, Y. S. Li, C. B. Xiang and S. Xianda, *J. Membr. Sci.*, 2006, **276**, 162–167.
12 C. Liao, J. Zhao, P. Yu, H. Tong and Y. Luo, *Desalination*, 2012, **285**, 117–122.
13 F. Shi, Y. Ma, J. Ma, P. Wang and W. Sun, *J. Membr. Sci.*, 2012, **389**, 522–531.
14 A. Bottino, G. Capannelli and A. Comite, *Desalination*, 2002, **146**, 35–40.
15 Z.-Q. Huang, F. Zheng, Z. Zhang, H.-T. Xu and K.-M. Zhou, *Desalination*, 2012, **292**, 64–72.
16 M. Yeow, Y. Liu and K. Li, *J. Membr. Sci.*, 2005, **258**, 16–22.
17 J. Hong and Y. He, *Desalination*, 2014, **332**, 67–75.
18 L. D. Chen, G. X. Jin, X. B. Wu, W. Z. Lang and D. Z. Sun, *Adv. Mater. Res.*, 2012, **356**, 2158–2161.
19 L. Y. Ng, A. W. Mohammad, C. P. Leo and N. Hilal, *Desalination*, 2013, **308**, 15–33.
20 G. R. Guillen, Y. Pan, M. Li and E. M. Hoek, *Ind. Eng. Chem. Res.*, 2011, **50**, 3798–3817.
21 V. Vatanpour, S. S. Madaeni, R. Moradian, S. Zinadini and B. Astinchap, *Sep. Purif. Technol.*, 2012, **90**, 69–82.
22 X. Zhao, J. Ma, Z. Wang, G. Wen, J. Jiang, F. Shi and L. Sheng, *Desalination*, 2012, **303**, 29–38.
23 J. Ma, Y. Zhao, Z. Xu, C. Min, B. Zhou, Y. Li, B. Li and J. Niu, *Desalination*, 2013, **320**, 1–9.
24 M. B. Thürmer, P. Poletto, M. Marcolin, J. Duarte and M. Zeni, *Mater. Res.*, 2012, **15**, 884–890.
25 J. Xu, Y. Tang, Y. Wang, B. Shan, L. Yu and C. Gao, *J. Membr. Sci.*, 2014, **455**, 121–130.
26 A. Ahmad, W. Ramli, W. Fernando and W. Daud, *Sep. Purif. Technol.*, 2012, **88**, 11–18.
27 P. Sukitpaneenit and T.-S. Chung, *J. Membr. Sci.*, 2009, **340**, 192–205.
28 Y. Teow, A. Ahmad, J. Lim and B. Ooi, *Desalination*, 2012, **295**, 61–69.
29 T. Kuilla, S. Bhadra, D. Yao, N. H. Kim, S. Bose and J. H. Lee, *Prog. Polym. Sci.*, 2010, **35**, 1350–1375.

30 Z. Wang, H. Yu, J. Xia, F. Zhang, F. Li, Y. Xia and Y. Li, *Desalination*, 2012, **299**, 50–54.
31 J. Zhang, Z. Xu, W. Mai, C. Min, B. Zhou, M. Shan, Y. Li, C. Yang, Z. Wang and X. Qian, *J. Mater. Chem. A*, 2013, **1**, 3101–3111.
32 B. M. Ganesh, A. M. Isloor and A. F. Ismail, *Desalination*, 2013, **313**, 199–207.
33 J. Lee, H.-R. Chae, Y. J. Won, K. Lee, C.-H. Lee, H. H. Lee, I.-C. Kim and J.-m. Lee, *J. Membr. Sci.*, 2013, **448**, 223–230.
34 Z. Xu, J. Zhang, M. Shan, Y. Li, B. Li, J. Niu, B. Zhou and X. Qian, *J. Membr. Sci.*, 2014, **458**, 1–13.
35 L. Yu, Y. Zhang, B. Zhang, J. Liu, H. Zhang and C. Song, *J. Membr. Sci.*, 2013, **447**, 452–462.
36 H. Zhao, L. Wu, Z. Zhou, L. Zhang and H. Chen, *Phys. Chem. Chem. Phys.*, 2013, **15**, 9084–9092.
37 J. Zhang, Z. Xu, M. Shan, B. Zhou, Y. Li, B. Li, J. Niu and X. Qian, *J. Membr. Sci.*, 2013, **448**, 81–92.
38 C. Zhao, X. Xu, J. Chen, G. Wang and F. Yang, *Desalination*, 2014, **340**, 59–66.
39 C. Zhao, X. Xu, J. Chen and F. Yang, *J. Environ. Chem. Eng.*, 2013, **1**, 349–354.
40 Y. Zhao, Z. Xu, M. Shan, C. Min, B. Zhou, Y. Li, B. Li, L. Liu and X. Qian, *Sep. Purif. Technol.*, 2013, **103**, 78–83.
41 G. Gonçalves, P. A. Marques, A. Barros-Timmons, I. Bdkin, M. K. Singh, N. Emami and J. Grácio, *J. Mater. Chem.*, 2010, **20**, 9927–9934.
42 A. Bottino, G. Camera-Roda, G. Capannelli and S. Munari, *J. Membr. Sci.*, 1991, **57**, 1–20.
43 C. Shi, L. Chen, Z. Xu, Y. Jiao, Y. Li, C. Wang, M. Shan, Z. Wang and Q. Guo, *Physica E*, 2012, **44**, 1420–1424.
44 N. Hamid, A. F. Ismail, T. Matsuura, A. Zularisam, W. Lau, E. Yuliwati and M. Abdullah, *Desalination*, 2011, **273**, 85–92.
45 D.-G. Kim, H. Kang, S. Han and J.-C. Lee, *J. Mater. Chem.*, 2012, **22**, 8654–8661.
46 D. R. Dreyer, S. Park, C. W. Bielawski and R. S. Ruoff, *Chem. Soc. Rev.*, 2010, **39**, 228–240.
47 M. El Achaby, F. Arrakhiz, S. Vaudreuil, E. Essassi and A. Qaiss, *Appl. Surf. Sci.*, 2012, **258**, 7668–7677.
48 Z. Jiang, G. Zheng, Z. Han, Y. Liu and J. Yang, *J. Appl. Phys.*, 2014, **115**, 204101.
49 M. Taniguchi, J. P. Pieracci and G. Belfort, *Langmuir*, 2001, **17**, 4312–4315.
50 Y.-F. Zhao, L.-P. Zhu, Z. Yi, B.-K. Zhu and Y.-Y. Xu, *J. Membr. Sci.*, 2013, **440**, 40–47.
51 E. Saljoughi, M. Amirilargani and T. Mohammadi, *Desalination*, 2010, **262**, 72–78.
52 E. Saljoughi and S. M. Mousavi, *Sep. Purif. Technol.*, 2012, **90**, 22–30.
53 M. Omidvar, S. mahmoud Mousavi, M. Soltanieh and A. A. Safekordi, *J. Environ. Health*, 2014, **12**, 1–10.
54 H. Susanto and M. Ulbricht, *J. Membr. Sci.*, 2009, **327**, 125–135.
55 B. Bhushan, Y. C. Jung and K. Koch, *Philos. Trans. R. Soc. London, Ser. A*, 2009, **367**, 1631–1672.
56 S. Schusser, S. Menzel, M. Bäcker, M. Leinhos, A. Poghossian, P. Wagner and M. Schöning, *Electrochim. Acta*, 2013, **113**, 779–784.
57 N. Pezeshk, D. Rana, R. Narbaitz and T. Matsuura, *J. Membr. Sci.*, 2012, **389**, 280–286.
58 M. Hashino, K. Hirami, T. Ishigami, Y. Ohmukai, T. Maruyama, N. Kubota and H. Matsuyama, *J. Membr. Sci.*, 2011, **384**, 157–165.
59 M.-Z. Li, J.-H. Li, X.-S. Shao, J. Miao, J.-B. Wang, Q.-Q. Zhang and X.-P. Xu, *J. Membr. Sci.*, 2012, **405**, 141–148.
60 S. Zinadini, A. A. Zinatizadeh, M. Rahimi, V. Vatanpour and H. Zangeneh, *J. Membr. Sci.*, 2014, **453**, 292–301.
61 V. Vatanpour, S. S. Madaeni, R. Moradian, S. Zinadini and B. Astinchap, *J. Membr. Sci.*, 2011, **375**, 284–294.